

pQCD phenomenology of elastic ed scattering

A.P. Kobushkin ^{a), b)} and Ya.D. Krivenko ^{c)}

^{a)} *N N Bogolyubov Institute for Theoretical Physics
Metrologicheskaya str. 14B, Kiev, 03143, Ukraine*

^{b)} *Research Center for Nuclear Physics, Osaka University (Suita Campus)
10-1, Mihogaoka Ibaraki Osaka 567-0047, Japan*

^{c)} *Institute for Nuclear Research
Prospekt Nauki 47, Kiev, 03028, Ukraine*

Abstract

Electron-deuteron elastic scattering data ($A(Q^2)$ and $B(Q^2)$ structure functions and polarization observables t_{20} , t_{21} and t_{22}) are fit with a model that respects asymptotic properties of pQCD at high momentum transfer. The data analysis shows that pQCD starts from $Q^2 = 3.5$ (GeV/c)². Predictions for the magnetic structure function $B(Q^2)$ and the polarization observables at high momentum transfer are given.

1 Introduction

In recent few years new data from TJNAF on the ed elastic scattering were reported. They include the electric structure function, $A(Q^2)$, measured with high precision up to $Q^2 = 6$ (GeV/c)² [1, 2] and measurements of tensor polarization observables, t_{20} , t_{21} and t_{22} , up to $Q^2 = 1.7$ (GeV/c)² [3].

This data, together with data on the magnetic structure function, $B(Q^2)$ [5], restrict the deuteron structure at scales where quark-gluon degrees of freedom are expected to become defrozen. For example, according to optimistic estimations pQCD should start from Q^2 of order of few (GeV/c)² [4]. It is nice that this prediction was confirmed by analysis of TJNAF data on $A(Q^2)$ at $Q^2 > 2$ (GeV/c)² [2].

For further conclusions one also should consider the spin structure of the deuteron from pQCD point of view. However data on polarization observables, as well as on $B(Q^2)$, correspond to $Q^2 \leq 2$ (GeV/c)², which is not

enough for pQCD. This is a typical intermediate region between nucleon-meson and quark-gluon pictures, where isobar configurations, meson exchange currents and constituent quark degrees of freedom are all important [6].

The purpose of this work is to investigate phenomenologically a smooth connection between nucleon-meson and pQCD regions and make predictions for $B(Q^2)$ and polarization observables at higher Q^2 , where pQCD should work. A parameterization which connects these two regions was proposed earlier by one of the authors (A.P. K.) and A.I. Syamtomov [7]. It assumes power fall off of helicity spin amplitudes at asymptotically high Q^2 coming from quark counting rules. A new analysis of the parameterization [7] which includes the recent TJNAF data was provided in [8]. Now we study logarithmic corrections to the power behavior. Such corrections are shown to be important for the structure function $A(Q^2)$ at the highest region of TJNAF energy [2].

The paper is organized as follows. In sect. 2 we discuss the general structure of helicity amplitudes for the elastic ed scattering in the light cone frame (LCF) and pQCD predictions for the helicity amplitudes at high Q^2 . Parameterization of helicity amplitudes which smoothly connects regions of low and high Q^2 is given in sect. 3. Then, in sect. 4, the data base and fitting procedure are summarized. Discussions and summary are given in sect. 5.

2 Helicity amplitudes and the deuteron form-factors

2.1 Helicity amplitudes in LCF

The main object of our analysis is helicity amplitudes of the $\gamma^* + d \rightarrow d$ transition

$$J_{\lambda' \lambda}^{\mu} = \langle p', \lambda' | j^{\mu} | p, \lambda \rangle, \quad (1)$$

where p and p' are momenta and λ and λ' are helicities of the deuteron in the initial and final states, respectively.

Due to gauge invariance, covariance and discrete symmetries only three of the 36 helicity amplitudes (1) are independent and one can choose different sets of independent helicity amplitudes. Direct calculations, however,

demonstrate that it is not so in dynamics at LCF [9]. This phenomena was shown to come from the incompatibility of transformation properties of approximate current and a deuteron wave function used in practical calculations [10, 11]. As a result a non-physical dependence on orientation of light-front plane appears. Thus the choice of the independent amplitudes becomes of great importance in pQCD calculations where LCF is often used.

First let us define LCF as a limiting reference system where the z -projection of the incoming and outgoing deuteron is close to infinity. In LCF the incoming and outgoing deuteron, p and p' , are given as follows

$$\begin{aligned} p^\mu &= \left(\mathcal{P} + \frac{M^2 + p_\perp^2}{4\mathcal{P}}, \vec{p}_\perp, \mathcal{P} - \frac{M^2 + p_\perp^2}{4\mathcal{P}} \right), \\ p'^\mu &= \left(\mathcal{P} + \frac{M^2 + p_\perp^2}{4\mathcal{P}}, -\vec{p}_\perp, \mathcal{P} - \frac{M^2 + p_\perp^2}{4\mathcal{P}} \right) \end{aligned} \quad (2)$$

with

$$p^+ \equiv p^0 + p^3 = 2\mathcal{P}, \quad p'^+ \equiv p'^0 + p'^3 = 2\mathcal{P}, \quad \mathcal{P} \gg M^2 + p_\perp^2 \quad (3)$$

(M is the deuteron mass). In this frame the momentum of the virtual photon is given by

$$q^\mu = (0, -2\vec{p}_\perp, 0), \quad \vec{p}_\perp = -\left(\frac{1}{2}Q, 0\right) \quad (4)$$

and polarization vectors for the deuteron in the initial and final states, respectively, read [9]

$$\begin{aligned} \varepsilon^\mu(\lambda = \pm 1, p) &= -\sqrt{\frac{1}{2}} \left(\pm \frac{p_\perp}{2\mathcal{P}}, \pm 1, i, \mp \frac{p_\perp}{2\mathcal{P}} \right), \\ \varepsilon^\mu(\lambda = 0, p) &= \frac{1}{M} \left(\mathcal{P} - \frac{M^2 - p_\perp^2}{4\mathcal{P}}, \vec{p}_\perp, \mathcal{P} + \frac{M^2 - p_\perp^2}{4\mathcal{P}} \right), \\ \varepsilon^\mu(\lambda' = \pm 1, p') &= -\sqrt{\frac{1}{2}} \left(\mp \frac{p_\perp}{2\mathcal{P}}, \pm 1, i, \pm \frac{p_\perp}{2\mathcal{P}} \right), \\ \varepsilon^\mu(\lambda = 0, p') &= \frac{1}{M} \left(\mathcal{P} - \frac{M^2 - p_\perp^2}{4\mathcal{P}}, -\vec{p}_\perp, \mathcal{P} + \frac{M^2 - p_\perp^2}{4\mathcal{P}} \right). \end{aligned} \quad (5)$$

Here we put $p_\perp \equiv \sqrt{\vec{p}_\perp^2}$. Using the standard expression for the e.m. current matrix element

$$J_{\lambda'\lambda}^\mu = - \left\{ G_1(Q^2) \varepsilon^*(\lambda', p') \varepsilon(\lambda, p) (p + p')^\mu + \right.$$

$$\begin{aligned}
& + G_2(Q^2)[\varepsilon^\mu(\lambda, p)(\varepsilon^*(\lambda', p')q) - \varepsilon^{*\mu}(\lambda', p')(\varepsilon(\lambda, p)q)] - \\
& - G_3(Q^2)(p + p')^\mu \frac{(\varepsilon^*(\lambda', p')q)(\varepsilon(\lambda, p)q)}{2M^2} \Big\} \quad (6)
\end{aligned}$$

one gets the following expressions for the plus-component

$$J_{00}^+ = p^+ \{ 2(1 - 2\eta)G_1 + 4\eta G_2 - 4\eta^2 G_3 \}, \quad (7)$$

$$J_{10}^+ = p^+ \{ 2\sqrt{2\eta}G_1 - \sqrt{2\eta}G_2 + 2\sqrt{2\eta}\eta G_3 \}, \quad (8)$$

$$J_{1-1}^+ = -p^+ \{ 2\eta G_3 \}, \quad (9)$$

$$J_{11}^+ = p^+ \{ 2G_1 + 2\eta G_3 \} \quad (10)$$

where $J_{\lambda\lambda'}^+ \equiv J_{\lambda\lambda'}^0 + J_{\lambda\lambda'}^3$. It is easy to show that they satisfy the so-called angular condition

$$(1 + 2\eta)J_{11}^+ + J_{1-1}^+ - 2\sqrt{2\eta}J_{10}^+ - J_{00}^+ = 0 \quad (11)$$

and thus there are only three independent helicity amplitudes between the J_{11}^+ , J_{1-1}^+ , J_{10}^+ and J_{00}^+ [9, 12].

Alternatively the angular condition (11) teaches us that even at pQCD extreme there appears (through dimensionless ratio $\eta = \frac{Q^2}{4M^2}$) an additional scale parameter $4M^2$, apart from the pQCD parameter Λ_{QCD}^2 .

2.2 The deuteron formfactors

The charge, $G_C(Q^2)$, magnetic, $G_M(Q^2)$, and quadrupole, $G_Q(Q^2)$, formfactors are connected with formfactors $G_1(Q^2)$, $G_2(Q^2)$ and $G_3(Q^2)$ as follows

$$\begin{aligned}
G_Q &= G_1 - G_2 + (1 + \eta)G_3, \\
G_C &= G_1 + \frac{2}{3}\eta G_Q, \\
G_M &= G_2. \quad (12)
\end{aligned}$$

Using (7)-(10) one expresses the $G_C(Q^2)$, $G_M(Q^2)$ and $G_Q(Q^2)$ in terms of any three helicity amplitudes $J_{\lambda\lambda'}^+$, for example

$$G_C = \frac{1}{2\mathcal{P}(2\eta + 1)} \left[\frac{3 - 2\eta}{6} J_{00}^+ + \frac{8}{3} \sqrt{\frac{\eta}{2}} J_{10}^+ + \frac{2\eta - 1}{3} J_{1-1}^+ \right], \quad (13)$$

$$\begin{aligned} G_M &= \frac{1}{2\mathcal{P}(2\eta+1)} \left[J_{00}^+ + \frac{(2\eta-1)}{\sqrt{2\eta}} J_{10}^+ - J_{1-1}^+ \right], \\ G_Q &= \frac{1}{2\mathcal{P}(2\eta+1)} \left[-\frac{1}{2} J_{00}^+ + \sqrt{\frac{1}{2\eta}} J_{10}^+ - \frac{\eta+1}{2\eta} J_{1-1}^+ \right]. \end{aligned}$$

In turn, the $A(Q^2)$ and $B(Q^2)$ structure functions and $t_{2i}(\theta, Q^2)$ polarizations read

$$A = G_C^2 + \frac{2}{3}\eta G_M^2 + \frac{8}{9}\eta^2 G_Q^2, \quad (14)$$

$$B = \frac{4}{3}\eta (1+\eta) G_M^2, \quad (15)$$

$$\begin{aligned} t_{20} &= -\frac{1}{\sqrt{2}\mathcal{S}} \left\{ \frac{8}{9}\eta^2 G_Q^2 + \frac{8}{3}\eta G_C G_Q + \frac{2}{3}\eta G_M^2 \left[\frac{1}{2} + (1+\eta)\operatorname{tg}^2 \frac{\theta}{2} \right] \right\}, \end{aligned} \quad (16)$$

$$t_{21} = \frac{2}{\sqrt{3}\mathcal{S} \cos \frac{\theta}{2}} \eta \left(\eta + \eta^2 \sin^2 \frac{\theta}{2} \right) G_M G_Q, \quad (17)$$

$$t_{22} = -\frac{1}{2\sqrt{3}\mathcal{S}} G_M^2, \quad (18)$$

where $\mathcal{S} = A^2 + B^2 \operatorname{tg}^2 \frac{\theta}{2}$.

2.3 pQCD predictions for the helicity amplitudes

From pQCD arguments one gets very simple rules to determine the power behavior of the helicity amplitudes J_{00}^+ , J_{10}^+ and J_{1-1}^+ [13, 14]. For example, it follows that the amplitude J_{00}^+ is a leading amplitude with an asymptotic fall off

$$J_{00}^+ \sim \left(\frac{\Lambda_{\text{QCD}}}{Q} \right)^{10} \quad (19)$$

up to logarithmic corrections. It was also argued that in LCF the helicity flip amplitudes J_{10}^+ and J_{1-1}^+ are suppressed as [15]

$$\frac{J_{10}^+}{J_{00}^+} \sim \frac{\Lambda_{\text{QCD}}}{Q}, \quad \frac{J_{1-1}^+}{J_{00}^+} \sim \left(\frac{\Lambda_{\text{QCD}}}{Q} \right)^2. \quad (20)$$

Similar considerations gives that

$$J_{11}^+ \sim J_{1-1}^+ \sim \left(\frac{\Lambda_{\text{QCD}}}{Q} \right)^2 J_{00}^+, \quad (21)$$

which agrees with the angular condition (11), but only at extremely high Q^2 , $Q^2 \gg 4M^2$.

In our analysis, following arguments of Ref. [15, 16], we consider the set J_{00}^+ , J_{10}^+ and J_{1-1}^+ as main amplitudes, where the behavior (19),(20) is regulated in the intermediate region only by the Λ_{QCD} . In turn, the amplitude J_{11}^+ must be determined from the angular condition (11) and depends on two scale parameters, Λ_{QCD} and $4M^2$.

3 Parameterization of helicity transition amplitudes

Following the idea of reduced nuclear amplitudes in QCD [17], we define the reduced helicity transition amplitudes g_{00} , g_{0+} and g_{+-} as follows:

$$\frac{1}{2\mathcal{P}} J_{\lambda,\lambda'}^+(Q^2) = G^2 \left(\frac{1}{4} Q^2 \right) g_{\lambda,\lambda'}(Q^2), \quad (22)$$

where $G(Q^2)$ is a three-quark-cluster (nucleon) formfactor. For the $G(Q^2)$ we assume dipole behavior $G(Q^2) = \left[1 + \frac{Q^2}{\mu^2} \right]^{-2}$, but with the μ^2 parameter different from that for a free nucleon 0.71 (GeV/c)^2 .

We consider separately two kinematical regions, large Q^2 region, $Q^2 > Q_0^2$, and low Q^2 region, $Q^2 < Q_0^2$. The parameter Q_0^2 is estimated to be of order of few $(\text{GeV}/c)^2$. Its exact value will be determined from a fit to experimental data.

pQCD predicts that at asymptotically high Q^2 the reduced transition amplitudes behave as follows

$$\begin{aligned} g_{00}^{(\text{asy})} &= \frac{N_1}{Q^2} \phi(Q^2), \quad g_{0+}^{(\text{asy})} = \frac{N_2}{Q^3} \phi(Q^2), \\ g_{+-}^{(\text{asy})} &= \frac{N_3}{Q^4} \phi(Q^2). \end{aligned} \quad (23)$$

In (24) the factor $\phi(Q^2)$ takes into account logarithmic corrections

$$\phi(Q^2) = \frac{[\alpha_s(Q^2)]^5}{[\alpha_s(Q^2/4)]^4} \frac{(\lg Q^2/\Lambda_{\text{QCD}}^2)^{\gamma^d}}{[\lg Q^2/(4\Lambda_{\text{QCD}}^2)]^{\gamma^N}} \quad (24)$$

and γ^d and γ^N are leading anomalous dimensions for the deuteron and the nucleon, respectively,

$$\gamma^d = \frac{6C_F}{5\beta}, \gamma^N = \frac{C_F}{2\beta}, \quad (25)$$

where $C_F = (n_c^2 - 1)/(2n_c)$, $\beta = 11 - \frac{2}{8}n_f$, $n_c = 3$ is number of quark colors and $n_f = 2$ is the number of flavors, $\alpha_s(Q^2) = \frac{4\pi}{\beta \ln Q^2/\Lambda_{\text{QCD}}^2}$ is the running quark-gluon coupling [4].

At $Q^2 \leq Q_0^2$ the following parameterization for the reduced amplitudes is assumed

$$\begin{aligned} \tilde{g}_{00} &= \sum_{n=1}^N \frac{a_n}{Q^2 + \alpha_n^2}, \quad \tilde{g}_{0+} = Q \sum_{n=1}^N \frac{b_n}{Q + \alpha_n}, \\ \tilde{g}_{+-} &= Q^2 \sum_{n=1}^N \frac{c_n}{Q^2 + \alpha_n^2}, \end{aligned} \quad (26)$$

where $\alpha_n^2 = [\alpha_0 + (n-1)m_0]^2$. One imposes the constraints (see, e.g., [7]):

$$\begin{aligned} \sum_{n=1}^N \frac{a_n}{\alpha_n^2} &= 1, \quad \sum_{n=1}^N \frac{b_n}{\alpha_n^2} = \frac{2 - \mu_d}{2\sqrt{2}M}, \\ \sum_{n=1}^N \frac{c_n}{\alpha_n^2} &= \frac{1 - \mu_d - Q_d}{2M^2} \end{aligned} \quad (27)$$

on the coefficients a_n , b_n and c_n to demand formfactor normalization at $Q^2 = 0$. In (28) $\mu_d = 0.857406 M/m_p$ is the deuteron magnetic moment in “deuteron magnetons” and $Q_d = 25.84$ is the deuteron quadrupole momentum in M^2/e .

The coefficients N_1 , N_2 and N_3 appearing in (27) cannot be calculated from pQCD and we determine them from the smooth connection of the two parametrizations at the point $Q^2 = Q_0^2$

$$g_{ij}^{(\text{asy})} = \tilde{g}_{ij}, \quad (28)$$

$$\begin{aligned}
\frac{d^2 g_{00}^{(\text{asy})}}{dQ^2} &= \frac{d^2 \tilde{g}_{00}}{dQ^2}, \\
\frac{d g_{0+}^{(\text{asy})}}{dQ} &= \frac{d \tilde{g}_{0+}}{dQ}, \\
\frac{d^2 g_{+-}^{(\text{asy})}}{dQ^2} &= \frac{d^2 \tilde{g}_{+-}}{dQ^2}.
\end{aligned}$$

4 Data base and fitting parameters

In our fit we use the following data: for $A(Q^2)$ from [1, 2, 18, 20, 21, 22, 23, 24, 25], for $B(Q^2)$ from [5, 20, 21, 26, 27], and polarization observables t_{20} from [3, 28, 29, 30, 31, 33, 34] and t_{22}, t_{21} from [31, 3]. But it must be noted that due to large errors the t_{22}, t_{21} data are practically not informative for the fit.

Q_0^2 was considered as a parameter of the model, but the QCD cutoff parameter Λ_{QCD} was fixed at 200 MeV. In (28) we chose $N = 4$, so that the model has 10 independent fit parameters. The fit parameters summarized in Table 1 were obtained with $\xi^2 = 399$ for 200 data points.

5 Discussion and summary

Figs. 1 and 2 display comparison of the model with $A(Q^2)$ data. The dotted line of Fig. 2 shows extrapolation of asymptotic behavior given by (24) to the region $1 \leq Q^2 < Q_0^2$. One concludes that for $A(Q^2)$ pQCD works from Q^2 -region between 1 and 2 GeV/c. Comparison with data for $B(Q^2)$ and the polarization observables are given on Figs. 3 — 5. One sees that for the magnetic formfactor pQCD should start from Q^2 between 2 and 3 GeV/c, but for the polarization observable it should start somewhat earlier, near 2 (GeV/c)².

Figs. 6 and 7 show results for the charge and quadrupole formfactors, $G_c(Q^2)$ and $G_q(Q^2)$.

In summary, we give a parametrization of the deuteron formfactors up to $Q^2 = 6$ (GeV/c)². Asymptotic behavior of the formfactors is dictated by quark counting rules and pQCD helicity rules. The model predicts behavior

of the magnetic structure function, $B(Q^2)$, at $Q^2 \geq 2.5$ $(\text{GeV}/c)^2$ which can be studied in future experiments.

References

- [1] L.C. Alexa et al., Phys. Rev. Lett. **82**, 1374 (1999).
- [2] D. Abbott et al., Phys. Rev. Lett. **82**, 1379 (1999).
- [3] D. Abbott et al., Phys. Rev. Lett. **84**, 5053 (2000).
- [4] S.J. Brodsky, C.-R. Ji and G.P. Lepage, Phys. Rev. Lett. **51**, 83 (1983).
- [5] P.E. Bosted et al., Phys. Rev. C **42**, 38 (1990).
- [6] E. Lomon, Phys. Rev. **C64**, 035204 (2001).
- [7] A.P. Kobushkin and A.I. Syamtomov, Phys. Atom. Nucl. **58**, 1477 (1995).
- [8] D. Abbott et al., Eur. Phys. J. A **7**, 421 (2000).
- [9] I.L. Grach and L.A. Kondratyuk, Sov. J. Nucl. Phys. **39**, 198 (1984).
- [10] V.A. Karmanov and A.V. Smirnov, Nucl.Phys. A **546**, 691 (1992).
- [11] V.A. Karmanov, Nucl. Phys. A **608**, 316 (1996).
- [12] P.L. Chung, F. Coester, B.D. Keister, and W.N. Polyzou, Phys. Rev. C **37**, 2000 (1988).
- [13] A.I. Vainshtein and V.I. Zakharov, Phys. Lett. B **72** 368 (1978).
- [14] C. Carlson and F. Gross, Phys. Rev. Lett. **53** 127 (1984).
- [15] S.J. Brodsky and J.R. Hiller, Phys. Rev. D **46**, 2141 (1992).
- [16] A.P. Kobushkin and A.I. Syamtomov, Phys. Rev. D **49**, 1637 (1994).
- [17] S.J. Brodsky and B.T. Chertok, Phys. Rev. Lett. **37**, 269 (1976); Phys. Rev. D **14**, 3003 (1976).
- [18] R.G. Arnold et al., Phys. Rev. Lett. **35**, 776 (1975).
- [19] D. Benaksas et al., Phys. Rev. **148**, 1327 (1966).
- [20] C.D. Buchanan and R. Yeadrian, Phys. Rev. Lett. **15**, 303 (1965).

- [21] R. Cramer et al., Z. Phys.. C **29**, 513 (1985).
- [22] D.J. Drikley and L.N. Hand., Phys. Rev. Lett. **9**, 521 (1962).
- [23] J.E. Elias et al., Phys. Rev. **9**, 521 (1969).
- [24] S. Gaster et al., Nucl. Phys. B **32**, 221 (1971).
- [25] S. Plachkov et al., Nucl. Phys. A **510**, 740 (1990).
- [26] S. Aufert et al., Phys. Rev. Lett. **54**, 649 (1985).
- [27] G.G. Simon et al., Nucl. Phys. A **364**, 285 (1981).
- [28] M. Bouwhuis et al., Phys. Rev. Lett. **82**, 3755 (1999).
- [29] V.F. Dmitriev et al., Phys. Lett. **157B**, 143 (1985).
- [30] M. Ferro-Luzzi et al., Phys. Rev. Lett. **77**, 2630 (1996).
- [31] M. Garcon et al., Phys. Rev. C **49**, 2516 (1994).
- [32] R. Gilman et al., Phys. Rev. Lett. **65**, 1733 (1990).
- [33] M. Schulze et al., Phys. Rev. Lett. **52**, 597 (1984).
- [34] B.B. Voitsekhovskii et al., JETP Lett. **43**, 733 (1986).

Table 1: Parameters of the model

α_0	0.2635	GeV
m_0	0.36864	GeV
a_1	$0.5373059 \cdot 10^{-1}$	GeV^{-2}
a_2	0.2836982	GeV^{-2}
a_3	from eqs. (28)	
a_4	from eqs. (27)	
b_1	$-9.898079 \cdot 10^{-1}$	
b_2	1.6950028	
b_3	from eqs. (28)	
b_4	from eqs. (27)	
c_1	-0.1074219	
c_2	$-0.7075449 \cdot 10^{-1}$	
c_3	from eqs. (28)	
c_4	from eqs. (27)	
Q_{QCD}^2	3.50120	GeV^2
μ^2	0.50959	GeV^2

Figure captions

Figure 1. Comparison of the model fit with data for $A(Q^2)$ at $Q^2 \leq 1$ (GeV/c) 2 . Data are from: filled triangle — [1], filled black — [2], filled diamond — [18], open down triangle — [19], open diamond — [20], black triangle — [21], open box — [22], open triangle — [23], open circle — [25].

Figure 2. Comparison of the model fit [solid] with data for $A(Q^2)$ at $Q^2 \geq 1$ (GeV/c) 2 . The dotted line is asymptotic behavior given by (24) extrapolated to lower transfer momentum. Symbols for data points are the same as in Fig. 1.

Figure 3. Comparison of the model fit [solid] with data for $B(Q^2)$. The dotted line is asymptotic behavior given by (24) extrapolated to lower transfer momentum. Data are from: filled circle — [5], diamond — [20], triangle — [21], circle — [26], star — [27].

Figure 4. Comparison of the model fit [solid] with data for t_{20} . The dotted line is asymptotic behavior given by (24) extrapolated to lower transfer momentum. Data are from: filled circle — [3], diamond — [28], triangle — [29], asterisk — [30], circle — [31], heartsuit — [32], down triangle — [33], star — [34].

Figure 5. Comparison of the model fit [solid] with data for t_{21} . The dotted line is asymptotic behavior given by (24) extrapolated to lower transfer momentum. Data are from: filled circle — [3], circle — [31].

Figure 6. Comparison of the model fit [solid] with data for t_{22} . The dotted line is asymptotic behavior given by (24) extrapolated to lower transfer momentum. Symbols for data points are the same as in Fig. 5.

Figure 7. Comparison of the model fit [solid lines] with data for $|G_c(Q^2)|$ (upper figure) and $G_q(Q^2)$ (lower figure). Data are from [8]. For the last two points the two solutions (filled and open points) are shown, see [8]. The dotted lines displays asymptotic behavior given by (24) extrapolated to lower transfer momentum.

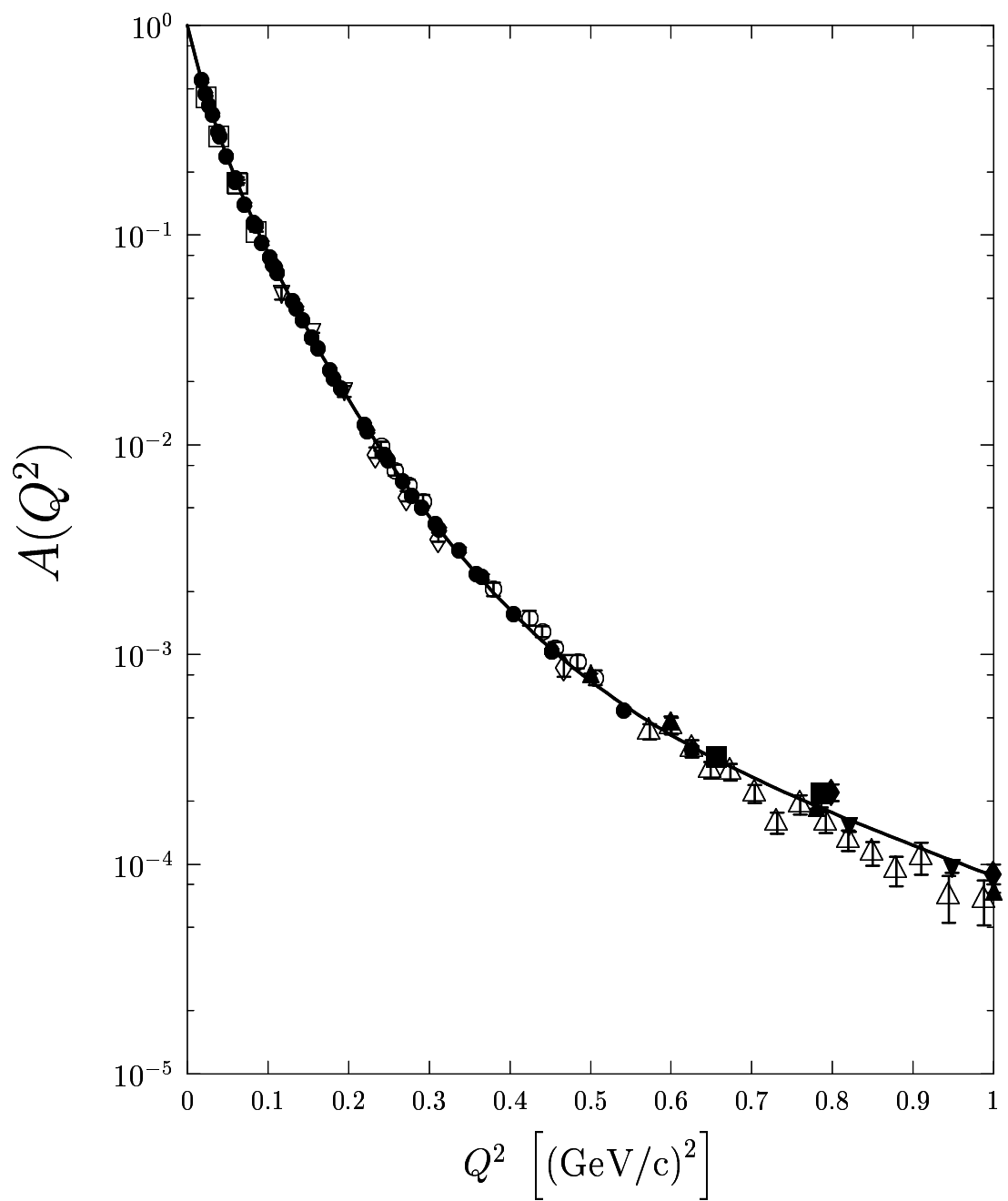


Fig. 1.

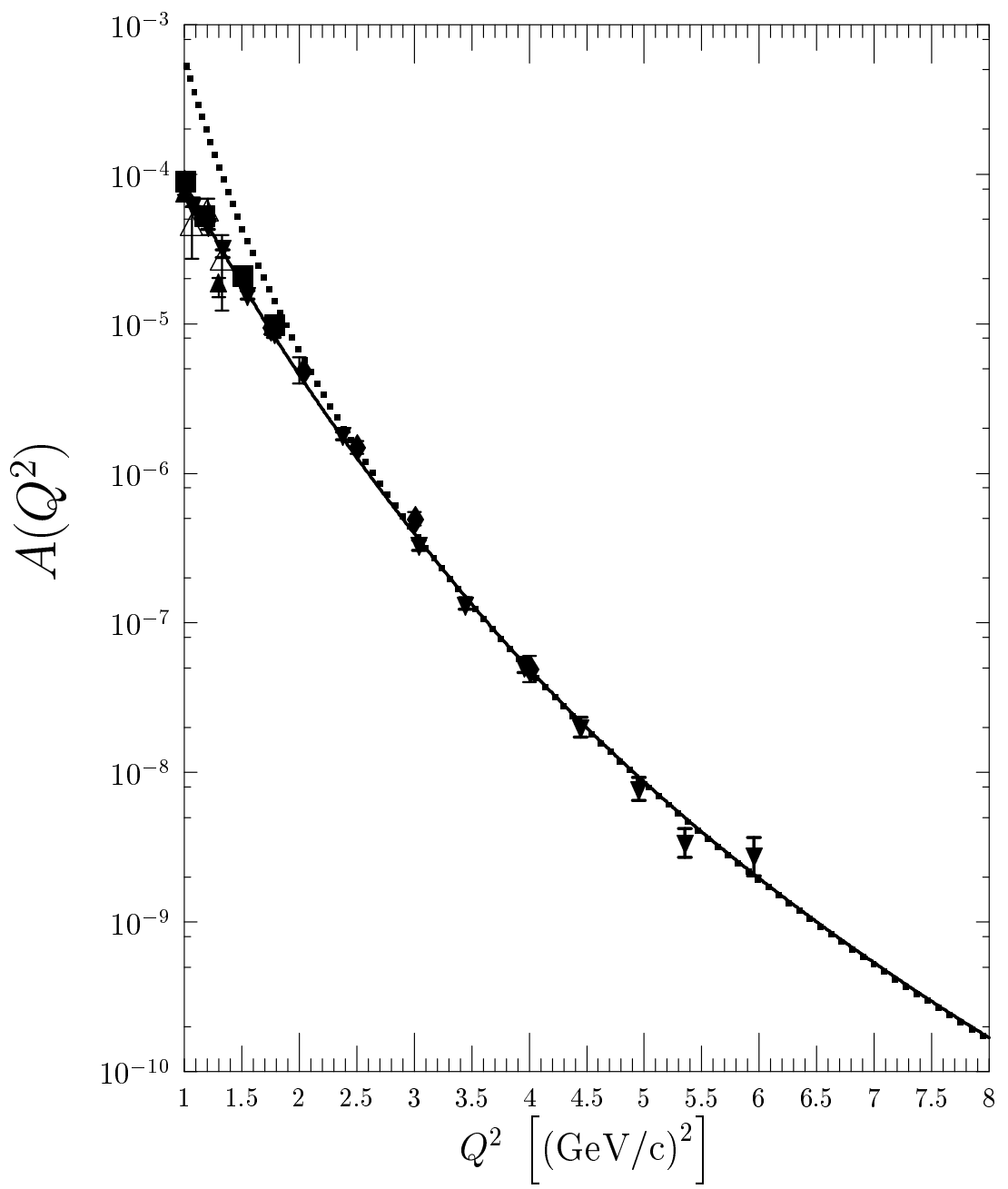


Fig. 2.

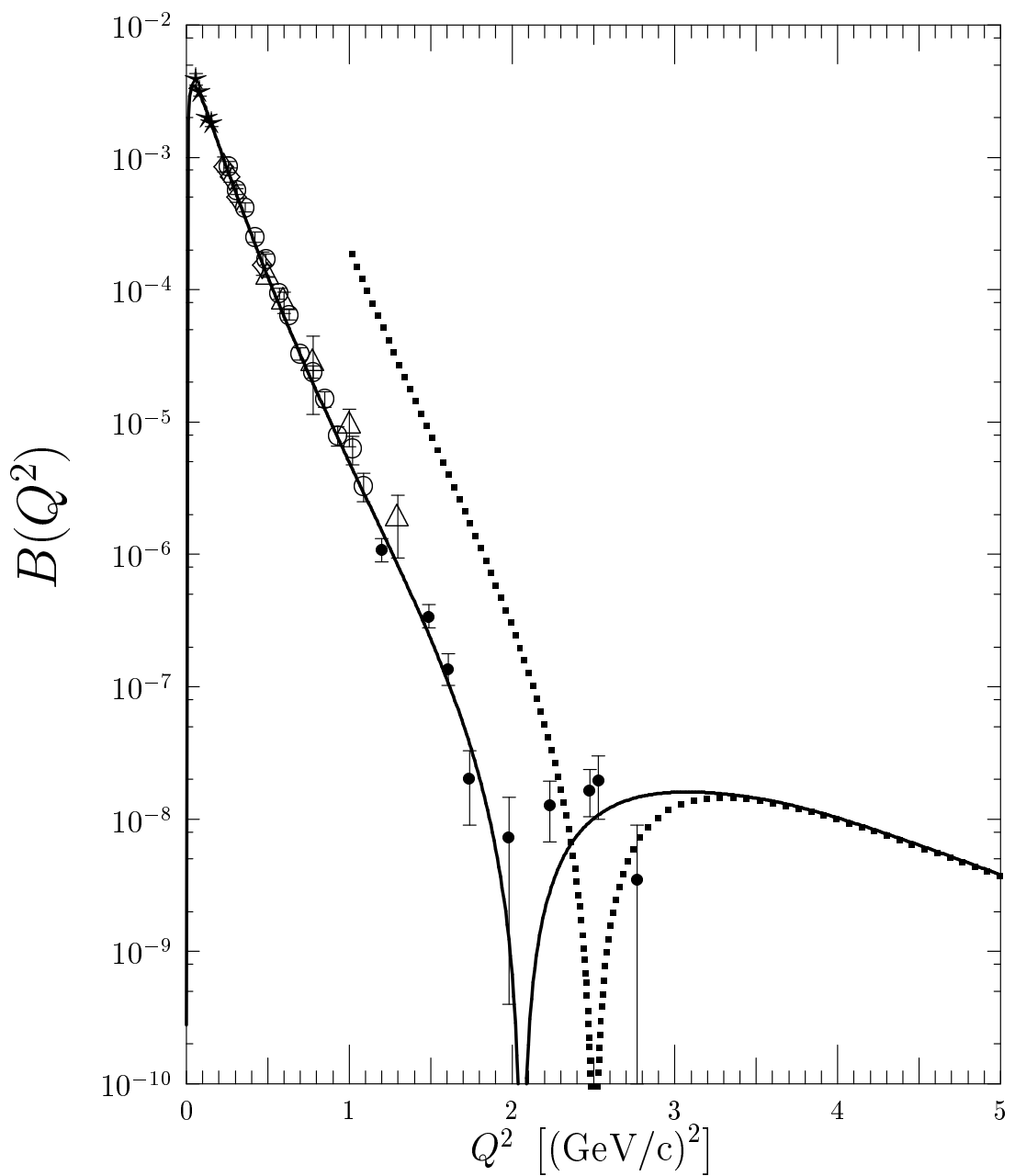


Fig. 3.

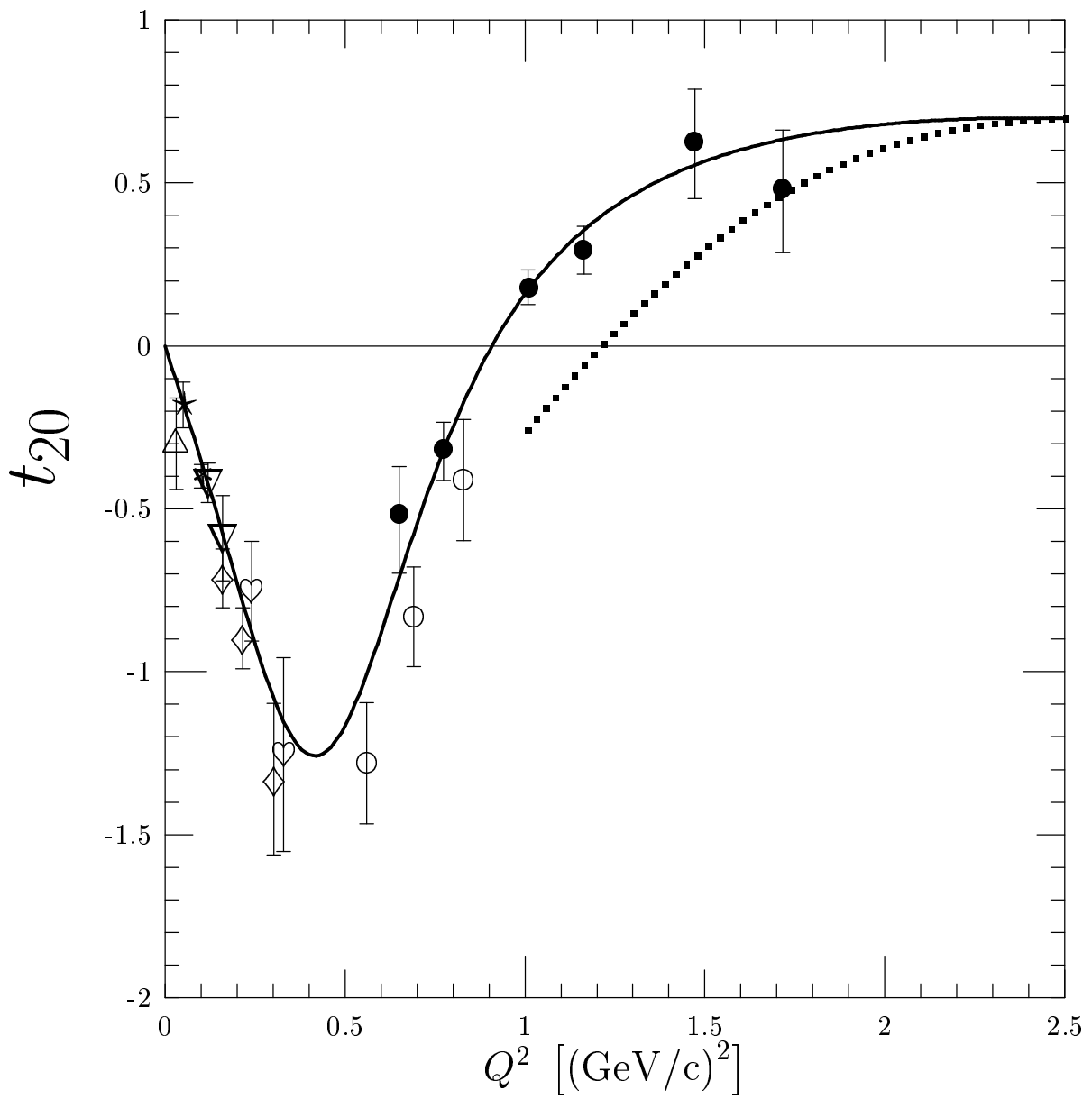


Fig. 4.

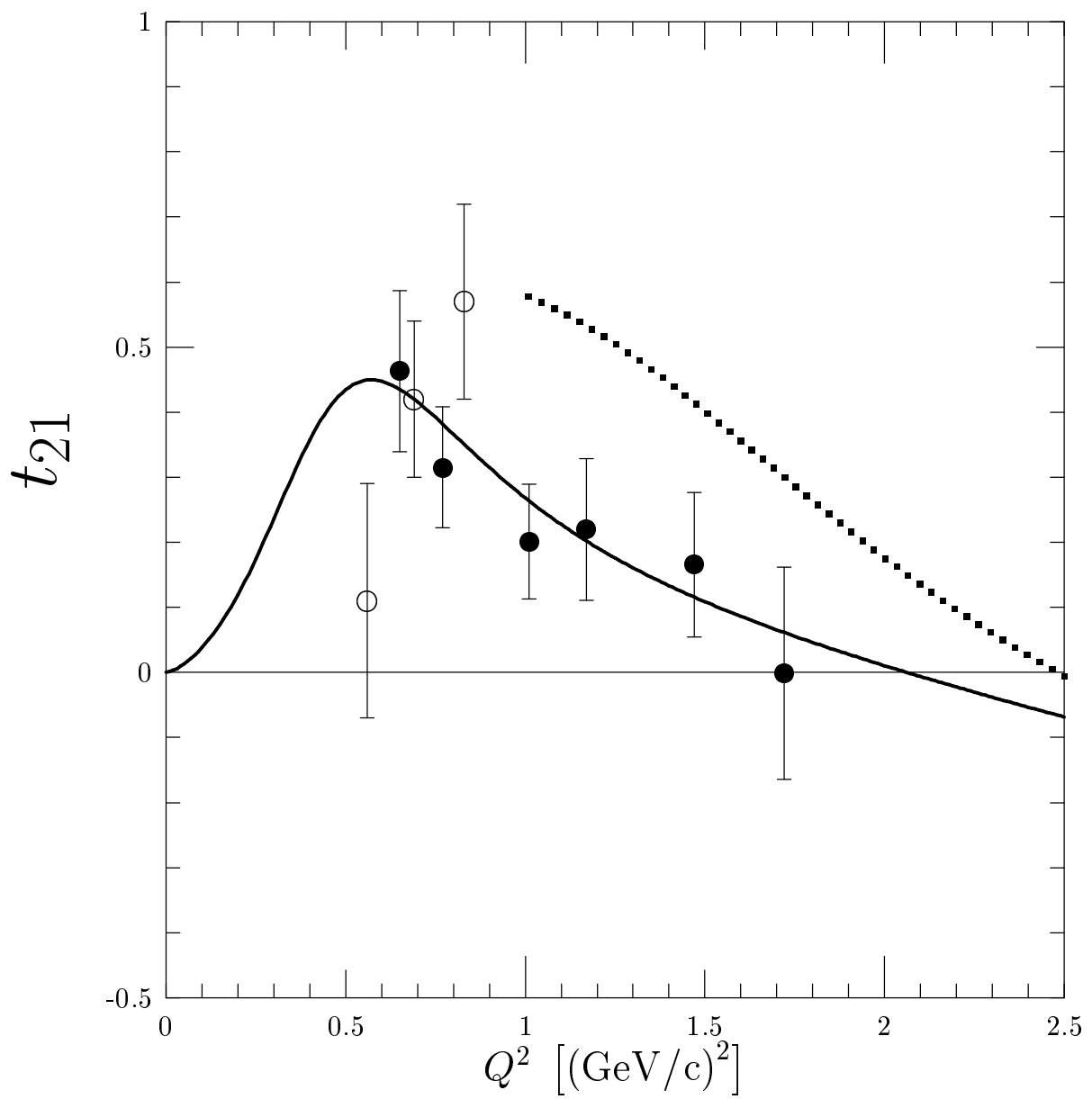


Fig. 5

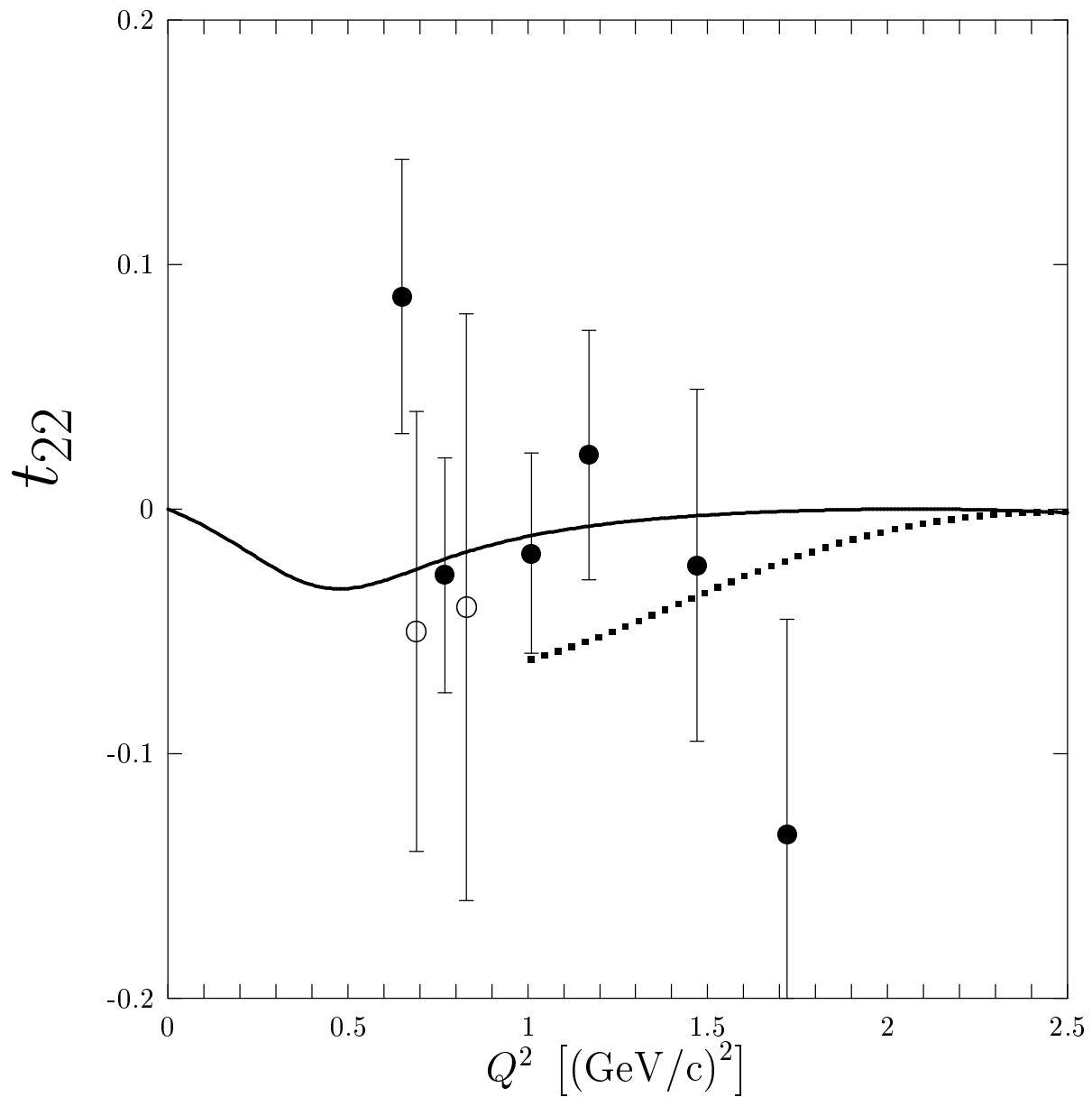


Fig. 6

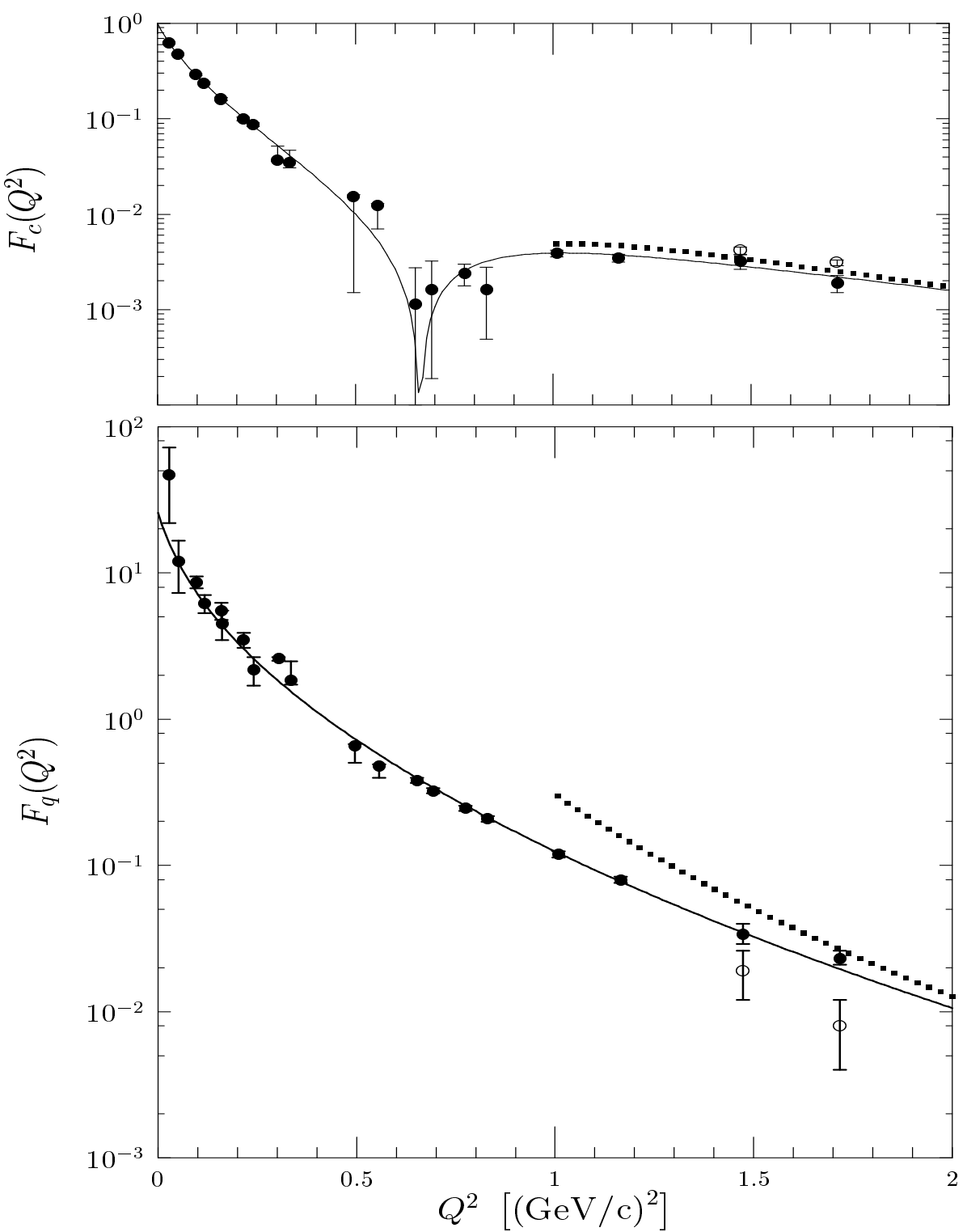


Fig. 7.